

# Model Predictive Control of Wind Turbines with Piecewise-Affine Power Coefficient Approximation

Arnold Sterle, Aaron Grapentin, Christian A. Hans and Jörg Raisch

**Abstract**—In this paper, an offset-free bilinear model predictive control approach for wind turbines is presented. State-of-the-art controllers employ different control loops for pitch angle and generator torque which switch depending on wind conditions. In contrast, the presented controller is based on one unified control law that works for all wind conditions. The inherent nonlinearity of wind turbines is addressed through a piecewise-affine approximation, which is modelled in a mixed-integer fashion. The presented controller is compared to a state-of-the-art baseline controller in a numerical case study using OpenFAST. Simulation results show that the presented controller ensures accurate reference power tracking. Additionally, damage equivalent loads are reduced for higher wind speeds.

## I. INTRODUCTION

The global goal of mitigating climate change remains a driving force for renewable energy sources. To achieve lower greenhouse gas emissions, renewable energy resources have to be widely deployed [1]. The globally installed wind power capacity has been increased to 837 GW in 2021 with 72 % being installed in China, the US, Germany, India and Spain [2]. On top, the cost of renewable energy has significantly declined over the last decade [3]. This trend is expected to continue in the upcoming years. The long-term operation and maintenance costs consist mainly of replacement costs [4]. Therefore, reducing wear becomes a key factor for the future development of wind power.

Two modes of wind turbine operation can be considered depending on wind conditions. At lower wind speeds, generated power shall be maximized. At higher wind speeds, generated power shall be curtailed such that a given reference power  $P_e^d$  is tracked, which is referred to as power tracking. Traditionally, control laws with individual loops for pitch and torque have been employed. These are switched depending on wind conditions (see, e.g., [5]–[7]). A multivariable control approach such as model predictive control (MPC) may improve control performance by considering pitch and torque interactions. However, formulating models and objectives that hold for large wind speed ranges remains a challenging objective which has previously been dealt with by switching cost functions [8], [9] or linear parameter varying models [10]. Potentially, such approaches may suffer from reduced control performance at operations close to the point of switching. Also, linear parameter varying models need to be

carefully designed to properly reflect the system dynamics for the entire operation range.

In this paper, an offset-free MPC scheme that is based on a mixed-integer bilinear program is presented. The controller combines pitch and torque control into a unified control law that holds for all wind conditions such that no switching is required. Additionally, it achieves improved power maximization capabilities while reducing loads at higher wind speeds. Our MPC scheme is thoroughly tested against a state-of-the-art controller in comprehensive numerical simulation case studies that employ OpenFAST [11]. Our MPC scheme proves to ensure accurate power tracking while reducing damage equivalent loads at higher wind speeds.

The paper is organized as follows. In Section II, a state model of a wind turbine is derived. Then, the MPC scheme is formulated in Section III. In Section IV, simulation results of the MPC approach and the baseline controller are presented and compared. Finally, conclusions are drawn in Section V.

### A. Preliminaries

The sets of positive integers, integers and real numbers are denoted by  $\mathbb{N}$ ,  $\mathbb{Z}$  and  $\mathbb{R}$ , respectively. The set of positive real numbers is denoted by  $\mathbb{R}^+$ . The set of nonnegative real numbers is denoted by  $\mathbb{R}_0^+$ . Inequalities between vector quantities are evaluated element-wise.

## II. MODEL

Similar to previous work (see, e.g., [10], [12]), we use a wind turbine model that is composed of three subsystems: aerodynamics, drive train and generator. The aerodynamic system, which consists of the wind turbine’s rotor hub and blades, converts wind into rotational motion. The drive train’s gearbox converts the rotor’s slow speed into the generator’s fast one. Finally, the generator converts mechanical into electrical power. In what follows, these parts will be discussed in detail.

### A. Aerodynamic subsystem

Wind passing through the rotor swept area  $\pi R^2$ , with radius  $R \in \mathbb{R}^+$ , exhibits a power of

$$P_{wind}(t) = m'V(t)^3, \quad (1)$$

with  $m' = \frac{1}{2}\rho\pi R^2$  where  $\rho \in \mathbb{R}^+$  denotes the air density and  $V(t) \in \mathbb{R}^+$  the rotor effective wind speed at time  $t \in \mathbb{R}$  [13, ch. 1]. For the case of  $V(t) = 0$ , the wind turbine is not operated. Hence this case is disregarded here. According to Betz’s law [13, ch. 1], the rotor can only convert a fraction of the wind power into rotational power  $P_r(t) \in \mathbb{R}$ . This

A. Sterle, A. Grapentin, J. Raisch and C. A. Hans are with Technische Universität Berlin, Control Systems Group, Germany {grapentin, sterle, raisch, hans}@control.tu-berlin.de J. Raisch is also with Science of Intelligence, Research Cluster of Excellence.

This work was partially supported by the German Federal Ministry for Economic Affairs and Climate Action (BMWK), project No. 03EE2036C.

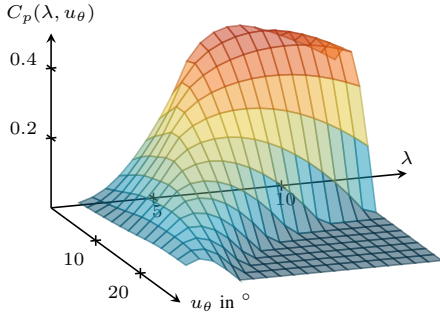


Fig. 1. Power coefficient  $C_p(\lambda, u_\theta)$  (data from [14]).

fraction is referred to as power coefficient  $C_p \in \mathbb{R}$  which depends on various parameters, such as rotor blade shape, material and weight. For a given turbine topology, it further depends on the wind speed's angle of attack on the rotor blades which changes with the blades' pitch angle  $u_\theta(t) \in \mathbb{R}$  and the tip-speed-ratio  $\lambda(t) \in \mathbb{R}^+$  which is given by

$$\lambda(t) = R \frac{\omega_r(t)}{V(t)}, \quad (2)$$

where  $\omega_r(t) \in \mathbb{R}^+$  denotes the rotor's angular velocity. For the case of  $\omega_r(t) = 0$ , the wind turbine is not operated. Hence this case is disregarded here. With  $u_\theta(t)$  and  $\lambda(t)$ , the power coefficient can be defined as

$$C_p(\lambda(t), u_\theta(t)) = \frac{P_r(t)}{P_{wind}(t)}. \quad (3)$$

Figure 1 depicts the power coefficient of a 3.4 MW wind turbine for different values of  $\lambda$  and  $u_\theta$ .

Combining (1) and (3) yields

$$P_r(t) = m' V(t)^3 C_p(\lambda(t), u_\theta(t)). \quad (4)$$

From this and (2), the aerodynamic rotor torque  $M_r(t) \in \mathbb{R}$  can be obtained as

$$M_r(t) = \frac{P_r(t)}{\omega_r(t)} = m' \frac{V(t)^3}{\omega_r(t)} C_p(\lambda(t), u_\theta(t)) \quad (5a)$$

$$= \underbrace{m' R}_{m} V(t)^2 \frac{C_p(\lambda(t), u_\theta(t))}{\lambda(t)}. \quad (5b)$$

### B. Drive train and gearbox subsystem

The wind turbine is modeled with a rigid drive train and gearbox, i.e., the generator angular velocity is  $\omega_g(t) = N_g \omega_r(t)$ , where  $N_g \in \mathbb{R}^+$  denotes the gearbox ratio. The dynamics are given by

$$J \dot{\omega}_r(t) = M_r(t) - \underbrace{N_g u_M(t)}_{M_g(t)}, \quad (6)$$

where  $u_M(t), M_g(t) \in \mathbb{R}$  denote the generator torque on the generator and rotor side, respectively and  $J \in \mathbb{R}^+$  the combined generator, rotor hub and blade inertia.

### C. Generator subsystem

The generator converts mechanical into electrical power with efficiency  $\eta \in (0, 1) \subset \mathbb{R}$ , i.e.,

$$P_e(t) = \eta \omega_g(t) u_M(t) = \eta N_g \omega_r(t) u_M(t). \quad (7)$$

### D. State model

From (2) and (5) to (7) a model with state  $\omega_r(t)$ , control input  $\mathbf{u}(t) = [u_\theta(t) \quad u_M(t)]^T$  and uncertain input  $V(t)$  of the form

$$\dot{\omega}_r(t) = \frac{m}{J} V(t)^2 \frac{C_p\left(\frac{R \omega_r(t)}{V(t)}, u_\theta(t)\right)}{R \frac{\omega_r(t)}{V(t)}} - \frac{N_g}{J} u_M(t), \quad (8a)$$

can be obtained. The output is the electrical power, i.e.,

$$P_e(t) = \eta N_g \omega_r(t) u_M(t). \quad (8b)$$

In what follows, a discrete-time model with sampling time  $T_s \in \mathbb{R}^+$  is used, i.e.,  $\omega_r(t)$  turns into  $\omega_r(kT_s)$ , with  $k \in \mathbb{Z}$ . For simplicity,  $\omega_r(k)$  is shorthand for  $\omega_r(kT_s)$ . Using the forward Euler method, the following discrete-time state model can be obtained from (8):

$$\begin{aligned} \omega_r(k+1) &= \omega_r(k) \\ &+ T_s \left( \frac{m}{J} V(k)^2 \frac{C_p\left(\frac{R \omega_r(k)}{V(k)}, u_\theta(k)\right)}{R \frac{\omega_r(k)}{V(k)}} - \frac{N_g}{J} u_M(k) \right) \end{aligned} \quad (9a)$$

$$P_e(k) = \eta N_g \omega_r(k) u_M(k). \quad (9b)$$

This model can now be used to derive a model predictive controller.

## III. MODEL PREDICTIVE CONTROLLER

In this section, an offset-free MPC approach is presented. It uses a model of a wind turbine based on (9) to find an optimal control trajectory that minimizes a cost function subject to constraints. First, a continuous piecewise-affine approximation of  $C_p$ , denoted as  $\hat{C}_p$ , is introduced. Then, a wind forecast model, a bilinear reformulation for (9a) and a disturbance observer are introduced and constraints presented. Finally, an MPC problem is formulated.

### A. Approximation of power coefficient

The design of the MPC scheme is based on (9a). The latter contains the power coefficient  $C_p(\lambda, u_\theta)$ , which is a nonlinear function of  $\lambda$  and  $u_\theta$ . To obtain a computationally tractable MPC formulation, a piecewise-affine approximation of the power coefficient is used. For this, we define  $N_R \in \mathbb{N}$  closed subsets  $S_j$ ,  $j \in [1, N_R] \subset \mathbb{N}$ , in  $\mathbb{R}^2$  of quadrilateral shape by systems of linear inequalities

$$\mathbf{A}_j [\lambda \quad u_\theta]^T \leq \mathbf{b}_j, \quad (10)$$

where  $\mathbf{A}_j \in \mathbb{R}^{4 \times 2}$  and  $\mathbf{b}_j \in \mathbb{R}^4$ . We choose  $\mathbf{A}_j, \mathbf{b}_j$  such that the corresponding sets  $S_j$ ,  $j \in [1, N_R]$  cover the relevant part of the  $\lambda$ - $u_\theta$ -plane and any interior point of  $S_j$ ,  $j \in [1, N_R]$  does not belong to any subset  $S_i$ ,  $i \neq j$ . We then define a piecewise affine approximation of  $C_p$ :

$$\hat{C}_p(\lambda, u_\theta) = a_j \lambda + b_j u_\theta + c_j \quad \text{if } [\lambda \quad u_\theta]^T \in S_j, \quad (11)$$

where  $a_j, b_j, c_j$  are chosen such that  $\hat{C}_p$  is continuous over all subsets  $S_j$ . An example of  $\hat{C}_p$  is depicted in Fig. 2.

Let the bounds  $\mathbf{M} \in \mathbb{R}^4$  and  $m_C, M_C \in \mathbb{R}$  be chosen such that  $\mathbf{A}_j [\lambda \quad u_\theta]^T \leq \mathbf{M}$  and  $m_C \leq a_j \lambda + b_j u_\theta + c_j \leq M_C$  for all  $j \in [1, N_R]$ . Motivated by [15], we use these bounds

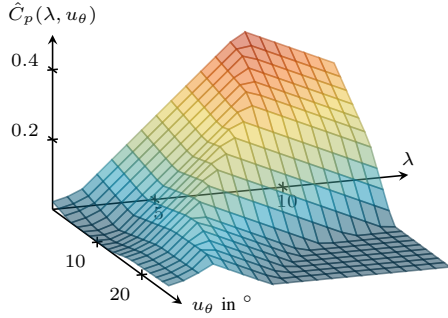


Fig. 2. Piecewise-affine approximation of  $\hat{C}_p$  for  $N_R = 9$ .

and additional binary variables  $\delta_j \in \{0, 1\}$  to obtain the following representation of the piecewise affine approximation

$$\hat{C}_p = \sum_{j=1}^{N_R} \hat{C}_{p,j}, \quad (12a)$$

$$1 = \sum_{j=1}^{N_R} \delta_j, \quad (12b)$$

$$\mathbf{A}_j [\lambda \quad u_\theta]^T \leq \delta_j \mathbf{b}_j + (1 - \delta_j) \mathbf{M}, \quad (12c)$$

$$\delta_j m_C \leq \hat{C}_{p,j} \leq \delta_j M_C, \quad (12d)$$

$$m_C(1 - \delta_j) \leq a_j \lambda + b_j u_\theta + c_j - \hat{C}_{p,j} \leq M_C(1 - \delta_j), \quad (12e)$$

for all  $j \in [1, N_R]$ .

*Remark 1:* One can distinguish between two cases for each subset  $j \in [1, N_R]$ :

- 1) For  $\delta_j = 0$ , (12d) becomes  $0 \leq \hat{C}_{p,j} \leq 0$ , i.e.,  $\hat{C}_{p,j} = 0$ . Equation (12e) becomes  $m_c \leq a_j \lambda + b_j u_\theta + c_j \leq M_c$  which does not impose any restrictions on  $\lambda$  and  $u_\theta$  by choice of  $m_c$  and  $M_c$ . Moreover, the upper bound in (12c) becomes  $\mathbf{M}$  which does not restrict  $[\lambda \quad u_\theta]^T$  either.
- 2) For  $\delta_j = 1$ , (12d) becomes  $m_C \leq \hat{C}_{p,j} \leq M_C$  which does not impose any restrictions on  $\hat{C}_{p,j}$ . Moreover, (12e) becomes equivalent to  $\hat{C}_{p,j} = a_j \lambda + b_j u_\theta + c_j$ . In (12c), the upper bound becomes  $\mathbf{b}_j$ , which turns this inequality into (10). Equation (12b) leads to  $\delta_i = 0 \forall i \in [1, N_R] \setminus \{j\}$ , and (12a) becomes  $\hat{C}_p = \hat{C}_{p,j} = a_j \lambda + b_j u_\theta + c_j$ .

With  $\hat{C}_p$ , a control oriented version of (9a) of the form

$$\begin{aligned} \omega_r(n+1|k) &= \omega_r(n|k) \\ &+ T_s \left( \frac{m}{J} V(n|k)^2 \frac{\hat{C}_p(n|k)}{R \frac{\omega_r(n|k)}{V(n|k)}} - \frac{N_g}{J} u_M(n|k) \right) \end{aligned} \quad (13)$$

can be derived  $\forall n \in [k, k + N_p]$ , where  $N_p \in \mathbb{N}$  denotes the controller prediction horizon. The notation  $\omega_r(n|k)$  refers to a prediction for time  $n$  performed at time  $k$ . Equation (13) can be used in the MPC to predict the system behaviour into the future.

### B. Wind speed forecast

To predict the system behaviour, a forecast of the wind speed  $V$  is required. In what follows, a widely employed persistence forecast [16, sec. 6.4] is used, i.e.,

$$V(n|k) = V(k). \quad (14)$$

$V(k)$  is assumed to be available through light detection and ranging (LIDAR) measurements or estimations (see, e.g., [17]–[19]). With (14), (13) becomes

$$\begin{aligned} \omega_r(n+1|k) &= \omega_r(n|k) \\ &+ T_s \left( \frac{m}{J} V(k)^2 \frac{\hat{C}_p(n|k)}{R \frac{\omega_r(n|k)}{V(k)}} - \frac{N_g}{J} u_M(n|k) \right). \end{aligned} \quad (15)$$

### C. Bilinear reformulation

The term

$$\frac{\hat{C}_p(n|k)}{R \frac{\omega_r(n|k)}{V(k)}} \quad (16)$$

in (15) includes a division of decision variables. Introducing  $z(n|k)$  by the bilinear expression

$$z(n|k) \omega_r(n|k) = \frac{V(k)}{R} \quad (17)$$

allows to state (16) as  $z(n|k) \hat{C}_p(n|k)$  which is bilinear as well. With (17), the prediction of the state can be written as

$$\begin{aligned} \omega_r(n+1|k) &= \omega_r(n|k) \\ &+ T_s \frac{mV(k)^2 z(n|k) \hat{C}_p(n|k) - N_g u_M(n|k)}{J}. \end{aligned} \quad (18)$$

The advantage of (17) and (18) over (15) is that they can be used in bilinear optimization problems which can be efficiently solved by a larger variety of available solvers.

### D. Offset-free control

Equation (18) is subject to model mismatch. Therefore, power tracking would not be offset free. Here, this mismatch is modelled by an input disturbance  $d_\omega(n|k)$ . Estimating this disturbance eliminates the offset [20]. Here, a persistence forecast is used, i.e.,

$$d_\omega(n|k) = d_\omega(k), \quad (19)$$

where  $d_\omega(k \leq 0) = 0$ . The signal is updated using the predicted  $\omega_r(k+1|k)$  and the measured  $\omega_r(k+1)$  via

$$d_\omega(k+1) = d_\omega(k) + L (\omega_r(k+1) - \omega_r(k+1|k)), \quad (20)$$

where  $L \in \mathbb{R}$  is the Luenberger observer gain (see [20]) which is found using a linearized wind turbine model [21]. Finally, the prediction used in the MPC can be posed as

$$\begin{aligned} \omega_r(n+1|k) &= \omega_r(n|k) + d_\omega(k) \\ &+ T_s \frac{mV(k)^2 z(n|k) \hat{C}_p(n|k) - N_g u_M(n|k)}{J}. \end{aligned} \quad (21)$$

### E. Constraints

The control input and its rate of change are bounded  $\forall k \in \mathbb{Z}, \forall n \in [k, k + N_p]$ , i.e.,

$$\underline{\mathbf{u}} \leq \mathbf{u}(n|k) \leq \bar{\mathbf{u}} \quad (22a)$$

$$\underline{\Delta \mathbf{u}} \leq \mathbf{u}(n|k) - \mathbf{u}(n-1|k) \leq \bar{\Delta \mathbf{u}} \quad (22b)$$

with  $\mathbf{u}(k-1|k) = \mathbf{u}(k-1)$  and bounds  $\underline{\mathbf{u}}, \bar{\mathbf{u}} \in \mathbb{R}^2$  and  $\underline{\Delta \mathbf{u}}, \bar{\Delta \mathbf{u}} \in \mathbb{R}^2$ . Additionally, to formulate a penalty for changes of  $\mathbf{u}$ , the constraint

$$-\epsilon_{\Delta u} \mathbf{u}(n|k) \leq \mathbf{u}(n|k) - \mathbf{u}(n-1|k) \leq \epsilon_{\Delta u} \mathbf{u}(n|k), \quad (23)$$

with  $\epsilon_{\Delta u}(n|k) \in \mathbb{R}^2$  is introduced. It can be used, for example, to reduce mechanical wear on the pitch actuators (see subsection III-F). To ensure feasibility, soft constraints on the state of the form

$$\underline{\omega}_r - \epsilon_\omega(n|k) \leq \omega_r(n|k) \leq \bar{\omega}_r + \epsilon_\omega(n|k), \quad (24)$$

are employed where  $\underline{\omega}_r, \bar{\omega}_r \in \mathbb{R}$  denote the lower and upper bound and  $\epsilon_\omega(n|k) \in \mathbb{R}$  is a slack variable. Both,  $\epsilon_\omega$  and  $\epsilon_{\Delta u}$  are nonnegative, i.e.,

$$0 \leq \epsilon_\omega(n|k) \quad (25a)$$

$$0 \leq \epsilon_{\Delta u}(n|k). \quad (25b)$$

The output power has a lower bound of zero, as no power shall be drawn from the grid, and upper bound  $P_e^d(k)$  which is an external input to the controller, i.e.,

$$0 \leq \eta N_g \omega_r(n|k) u_M(n|k) \leq P_e^d(k). \quad (26)$$

Thus, if enough wind power is available, then the output power should track  $P_e^d(k)$ .

#### F. Problem formulation

All decision variables at prediction step  $n$  are collected in

$$\mathbf{x}(n|k) = [\omega_r(n|k) \quad \mathbf{u}(n|k)^T \quad \hat{C}_p(n|k) \quad z(n|k) \quad \epsilon_\omega(n|k) \quad \epsilon_{\Delta u}(n|k)^T \quad \delta_1(n|k) \dots \delta_{N_R}(n|k)]^T. \quad (27)$$

The decision variables over prediction horizon  $N_p$  are collected in

$$\mathbf{X}(k) = [\mathbf{x}(k|k)^T \dots \mathbf{x}(k + N_p - 1|k)^T \omega_r(k + N_p|k)^T]. \quad (28)$$

The cost function to be minimized at step  $k$  is

$$\ell(\mathbf{X}(k)) = \sum_{n=k}^{k+N_p} ((-\eta N_g \omega_r(n|k) u_M(n|k) + q_\omega \epsilon_\omega(n|k) + \mathbf{q}_{\Delta u}^T \epsilon_{\Delta u}(n|k)) \gamma^{n-k}). \quad (29)$$

Here,  $q_\omega \in \mathbb{R}^+$  and  $\mathbf{q}_{\Delta u} \in \mathbb{R}^2$ ,  $\mathbf{q}_{\Delta u} > 0$  are weights. Moreover,  $\gamma \in (0, 1)$  is used to emphasize decisions in the near future. Hence control aims at rewarding output power  $P_e(k) = \eta N_g \omega_r(k) u_M(k)$  and at penalizing  $\epsilon_\omega(k)$  and  $\epsilon_{\Delta u}$ . Together with (26), (29) yields a controller which maximizes  $P_e(k)$  while ensuring that  $P_e^d(k)$  is not exceeded. Finally, the following MPC problem for a wind turbine can be formulated.

*Problem 1:*

$$\min_{\mathbf{X}(k)} \ell(\mathbf{X}(k))$$

subject to

$$\omega_r(n+1|k) = \omega_r(n|k) + d_\omega(k) + T_s \frac{mV(k)^2 z(n|k) \hat{C}_p(n|k) - N_g u_M(n|k)}{J},$$

as well as (12), (17) and (22) to (26)  $\forall n \in [k, k + N_p]$ , with measured  $\omega_r(k|k) = \omega_r(k)$  and  $u(k-1|k) = u(k-1)$ .

The solution for  $\mathbf{u}(k|k)$  obtained by solving Problem 1 is used to actuate the system at time  $k$ . At time  $k+1$ , a new measurement  $\omega_r(k+1|k+1) = \omega_r(k+1)$  is obtained,  $d_\omega(k+1)$  and  $V(k+1)$  are updated and the optimization process is repeated.

## IV. CASE STUDY

In this section, our MPC scheme is compared to the baseline controller from [21]. For this comparison the IEA 3.4-MW land-based wind turbine from [14] is used. The parameters for the MPC can be found in Table I. Additionally, the parameters for  $\hat{C}_p$  can be found in [22]. The MPC algorithm is implemented in MATLAB [23] using the Yalmip toolbox [24]. Gurobi [25] is used to numerically solve Problem 1. Unit tests have been deployed to ensure that the obtained results are correct. All simulations are conducted on a small server with an Intel® Xeon® E5-1620 v2 processor @3.70 GHz with 4 CPU cores and 32 GB RAM. A sampling time  $T_s = 3$  s and a prediction horizon of 6 samples are considered. For each simulation, the first 2 min are omitted to disregard startup effects of the simulation tool OpenFAST. All simulations were conducted with nonzero turbulence intensities (see [26]). In detail, a turbulence intensity of 9% was considered.

In Fig. 3, simulation results obtained with the MPC and the baseline controller are depicted for an average wind speed of 8 m/s. For this wind speed, the available power is below the demanded one and thus, the generated power is maximized. Note, that while the baseline controller keeps the rotor speed at a constant level, the MPC changes the rotor speed with the power reference. However, this has no effect on the power maximization as the generator torque counteracts this effect. Moreover, the pitch angle is kept constant for both controllers to keep the power coefficient at its maximum value. From Fig. 1, it becomes apparent that the power coefficient has a maximum plateau rather than a singular maximum point. Hence, different pitch angles may lead to the same maximum power. The general behaviour of the MPC in this operating region is currently being further investigated.

In Fig. 4, simulation results for an average wind speed of 16 m/s are shown. For this wind speed, the available power exceeds the demanded one and thus needs to be curtailed. Both controllers track the reference well. One notable difference is that the MPC approach employs less control action which becomes evident when observing the pitch angle. Consequently, the wear on the pitch actuators is reduced which may reduce long term maintenance cost.

TABLE I  
MPC PARAMETERS

Parameter	Value
$\underline{\omega}_r$	0.3979 rad/s
$\bar{\omega}_r$	1.2305 rad/s
$\underline{\mathbf{u}}$	[0.5263° 0 kN m] <sup>T</sup>
$\bar{\mathbf{u}}$	[26° 31.5751 kN m] <sup>T</sup>
$\Delta \underline{\mathbf{u}}$	[-21° -45 kN m] <sup>T</sup>
$\Delta \bar{\mathbf{u}}$	[21° 45 kN m] <sup>T</sup>
$L$	0.5
$T_s$	3 s
$N_p$	6
$q_\omega$	10 <sup>5</sup> s/rad
$q_{\Delta u}$	[1/° 1/kNm] <sup>T</sup>
$\gamma$	0.99

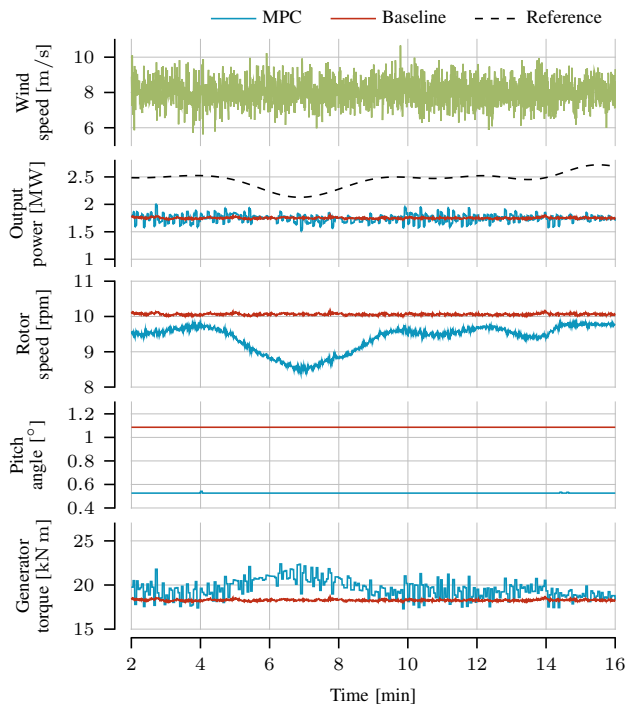


Fig. 3. Power maximization for a 8 m/s.

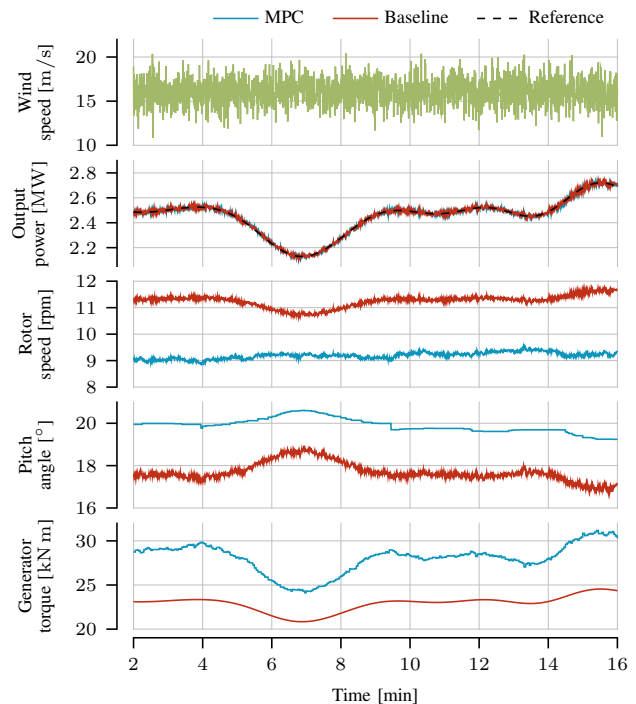


Fig. 4. Power tracking for an average wind speed of 16 m/s.

Moreover, the MPC approach employs a higher generator torque yielding a lower rotor speed, which reduces noise.

In Fig. 5, an operation where the average wind speed transitions back and forth between 6 and 16 m/s is shown. Both controllers are maximizing the output power for lower wind speeds which do not allow a generation of the reference power. At higher wind speeds, both controllers track the reference power. However at changing wind conditions, the baseline controller yields an undesired overshoot. The MPC on the contrary, leads to a better reference tracking at this point. When the wind speed decreases both controllers try to maximize the generated power. Briefly, the MPC approach tries to keep generating the reference power before reaching a new operating point. This different approach leads to higher energy production as in the depicted period from 10.5 min to 12 min, the turbine generates roughly 5.6% more energy with the MPC approach.

Fig. 6 shows the relative change for different damage equivalent loads (DELs) when using the MPC approach compared to the baseline controller. They are computed using the rainflow algorithm [27] and estimated for a 20 years life period [28]. While some DELs slightly increase at lower wind speeds, all of them significantly decrease at higher wind speeds when the MPC approach is employed. Therefore, the MPC approach can reduce mechanical wear and thus replacement costs for operations with higher wind speeds.

Finally, the solver time of the MPC approach is evaluated. Fig. 7 depicts boxplots of the solver times for simulations with different wind speeds. It can be observed that the solver time is smaller for higher wind speeds. However at all times, it stays below the sampling time of 3 s which renders the

controller applicable for wind turbine applications.

## V. CONCLUSION

In this paper, a model predictive wind turbine controller with a piecewise-affine power coefficient approximation was presented. It was shown that this approach favourably compares with state-of-the-art controllers in terms of power tracking accuracy, energy production and load reduction.

The developed MPC scheme provides a good basis for a variety of possible future extensions: the controller can, for example, be extended to account explicitly for damage equivalent loads by incorporating them in its cost function. A persistent feasibility analysis shall be performed to ensure safe real-world application of the controller. Additionally, the complexity of the MPC scheme shall be reduced to decrease the solver time, which enables a larger prediction horizon. Making the MPC compute references and moving the actual control to a low layer controller could achieve this. Another approach could be a modified construction of  $\hat{C}_p$  such that less probable areas in the  $\lambda-u_\theta$ -plane are approximated with less subsets and more probable areas with more subsets.

## REFERENCES

- [1] O. Edenhofer, R. Pichs-Madruga, Y. Sokona, K. Seyboth, P. Matschoss, S. Kadner, T. Zwickel, P. Eickemeier, G. Hansen, S. Schlömer *et al.*, "IPCC special rep. on renew. energy sources and climate change mitigation," *Prepared By Working Group III of the IPCC, Cambridge University Press, Cambridge, UK*, 2011.
- [2] Global Wind Energy Council, "Global wind report 2021," 2021.
- [3] IRENA, "Renewable power generation costs in 2020," *International Renewable Energy Agency*, 2021.
- [4] W. Vachon, "Long-term o&m costs of wind turbines based on failure rates and repair costs," in *Proceedings WINDPOWER, AWEA annu. conference, Portland, OR, 2002*, pp. 2–5.



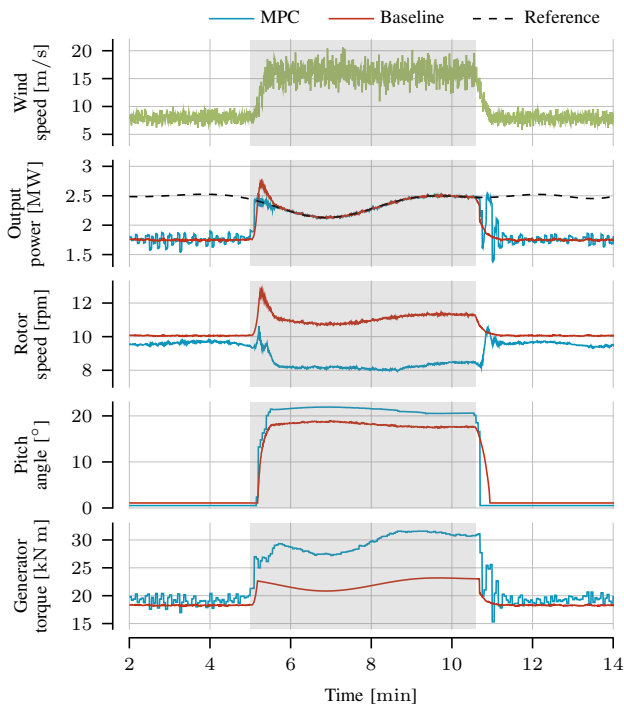


Fig. 5. Controller performance for varying wind speeds.

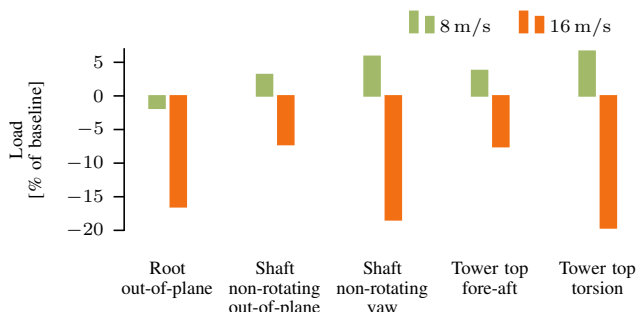


Fig. 6. Damage equivalent loads at different wind speeds.

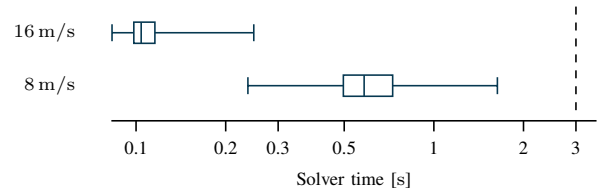


Fig. 7. Distribution of solve times at different average wind speeds. The dashed line marks the sampling time of the MPC approach.

- [5] J. Aho, A. Buckspan, J. Laks, P. Fleming, Y. Jeong, F. Dunne, M. Churchfield, L. Pao, and K. Johnson, "A tutorial of wind turbine control for supporting grid frequency through active power control," in *2012 ACC*, 2012, pp. 3120–3131.
- [6] K. Kim, H.-G. Kim, C. jin Kim, I. Paek, C. L. Bottasso, and F. Campagnolo, "Design and Validation of Demanded Power Point Tracking Control Algorithm of Wind Turbine," *International J. of Precision Engineering and Manufacturing-Green Technology*, vol. 5, no. 3, pp. 387–400, 2018.
- [7] O. Apatu and D. Oyedokun, "An overview of control techniques for wind turbine systems," *Scientific African*, vol. 10, p. e00566, 2020.
- [8] D. Schlipf, D. J. Schlipf, and M. Kühn, "Nonlinear model predictive control of wind turbines using LIDAR," *Wind Energy*, vol. 16, no. 7, pp. 1107–1129, 2012.
- [9] M. Mirzaei, M. Soltani, N. K. Poulsen, and H. H. Niemann, "An MPC approach to individual pitch control of wind turbines using uncertain LIDAR measurements," in *ECC*, 2013, pp. 490–495.
- [10] A. Morsi, H. S. Abbas, and A. M. Mohamed, "Model predictive control of a wind turbine based on linear parameter-varying models," in *IEEE CCA*, 2015, pp. 318–323.
- [11] B. Jonkman, R. M. Mudafort, A. Platt, E. Branlard, M. Sprague, J. Jonkman, HaymanConsulting, G. Vijayakumar, M. Buhl, H. Ross, P. Bortolotti, M. Masciola, Shreyas Ananthan, M. J. Schmidt, J. Rood, Rdamiani, Nrmendoza, Sinolonghai, M. Hall, Ashesh2512, Kshaler, K. Bendl, Pschuenemann, Psakievich, Ewquon, Mattrphillips, N. KUSUNO, Alvarogonzalezsalcedo, T. Martinez, and Rcorniglion, "OpenFAST/openfast: OpenFAST v3.1.0," 2022.
- [12] A. Merabet, J. Thongam, and J. Gu, "Torque and pitch angle control for variable speed wind turbines in all operating regimes," in *10th IEEEIC*. IEEE, 2011, pp. 1–5.
- [13] M. Hansen, *Aerodynamics of Wind Turbines*. Routledge, 2015.
- [14] P. Bortolotti, H. C. Tarres, K. Dykes, K. Merz, L. Sethuraman, D. Verelst, and F. Zahle, "IEA wind task 37 on systems engineering in wind energy – wp2.1 reference wind turbines," NREL/TP-73492, International Energy Agency, Tech. Rep., 2019.
- [15] A. Bemporad and M. Morari, "Control of systems integrating logic, dynamics, and constraints," *Automatica*, vol. 35, no. 3, pp. 407–427, 1999.
- [16] C. A. Hans, "Operation control of islanded microgrids," 2021.
- [17] G. Hafidi and J. Chauvin, "Wind speed estimation for wind turbine control," *IEEE International CCA*, 2012.
- [18] J. Schreiber, C. L. Bottasso, and M. Bertelè, "Field testing of a local wind inflow estimator and wake detector," *Wind Energy Science*, vol. 5, no. 3, pp. 867–884, 2020.
- [19] V. S. Nasrabad, A. Hajnayeb, and Q. Sun, "Effective wind speed estimation based on a data-driven model of wind turbine tower deflection," *Proceedings of the Institution of Mechanical Engineers, Part C: Journal of Mechanical Engineering Science*, vol. 236, no. 2, pp. 795–810, 2021.
- [20] G. Pannocchia, M. Gabiccini, and A. Artoni, "Offset-free MPC explained: novelties, subtleties, and applications," *IFAC-PapersOnLine*, vol. 48, no. 23, pp. 342–351, 2015.
- [21] A. Grapentin, A. Sterle, J. Raisch, and C. A. Hans, "LQ Optimal Control for Power Tracking Operation of Wind Turbines," *Preprint*, 2022, arXiv:2211.07690.
- [22] A. Sterle, "Model predictive control of wind turbines with piecewise affine power coefficient," 2023. [Online]. Available: <http://dx.doi.org/10.5281/zenodo.7593989>
- [23] MATLAB, *version 9.11.0 (R2021b)*. Natick, Massachusetts: The MathWorks Inc., 2021.
- [24] J. Löfberg, "Yalmip : A toolbox for modeling and optimization in matlab," in *In Proceedings of the CACSD Conference*, 2004.
- [25] Gurobi Optimization, LLC, "Gurobi Optimizer Reference Manual," 2022. [Online]. Available: <https://www.gurobi.com>
- [26] C. MacEachern and Ilhami Yildiz, "1.16 wind energy," in *Comprehensive Energy Systems*, Oxford, 2018, pp. 665–701.
- [27] N. E. Dowling, "Fatigue Failure Predictions for Complicated Stress Strain Histories," University of Illinois at Urbana-Champaign, Tech. Rep., 1971.
- [28] T. Burton, N. Jenkins, D. Sharpe, and E. Bossanyi, *Wind Energy Handbook*. John Wiley & Sons, 2011.